AAS 17-464

REACHABILITY SUBSPACE EXPLORATION USING CONTINUATION METHODS

Julian Brew[*], Marcus J. Holzinger[†], Stefan Schuet[‡]

Reachability manifold computation suffers from the curse of dimensionality and for large state spaces is computationally intractable. This paper examines the use of continuation methods to address this issue by formulating the reachability subspace manifold calculation into a number of initial value problems. As a result of computing the reachability manifold for a subspace of interest, an exponential improvement in computational cost occurs. This concept is applied to a position subspace reachability problem of a spacecraft in a Keplerian orbit under maximum thrust constraints. Future work includes a comparison of the proposed method with computing reachability manifolds using viscosity solutions of the Hamilton Jacobi Bellman partial differential equation.

INTRODUCTION

Reachability manifolds are volumes in state-space that can be reached given an integration constraint such as a final time horizon. The computation of reachability manifolds has been applied to problems such as vehicle collision avoidance, operational safety planning, and capability demonstration. The theory supporting reachability has been discussed in controls literature as it's derived from optimal control theory.[1,2,3] Computing the reachability manifold for a system involves solving the Hamilton-Jacobi-Bellman partial differential equation (HJB PDE). Commonly, minimum time reachability allows for safety and capability analyses to be conducted. These minimum time reachability manifolds are determined by computing viscosity solutions of the HJB PDE. The zero level sets of the value function over time represent the boundary of the minimum time reachability manifold.[4,5] This solution approach has many parallels with computational fluid dynamics (CFD) problems in which space and time are discretized into a grid and the governing partial differential equations are solved numerically.[4,6] There are many analogous problems that require performance indices besides minimum time, such as minimum fuel or minimum control effort. Holzinger et al. extended the typical optimal reachability framework to allow for integration constraints other than fixed total time and performance indices other than minimum time.[7]

The computation of reachability manifolds are generally intractable for state space dimensions greater than $n = 4$. To reduce the computation burden incurred by these problems, over/under-approximations for the reachability set have been developed. Polytopic, ellipsoidal, and support function approaches have been proposed and applied to several problems.[1,8,9,10,11] However, the

[*]Graduate Student, The Guggenheim School of Aerospace Engineering, Georgia Institute of Technology, Atlanta, GA 30332, AIAA Student Member

[†]Assistant Professor, The Guggenheim School of Aerospace Engineering, Georgia Institute of Technology, Atlanta, GA 30332, AIAA Senior Member

[‡]Research Engineer, NASA Ames Research Center, Moffet Field, CA 94035

curse of dimensionality continues to hamper the computation of the reachability manifolds as the required computation typically scales as an exponential of the problem dimension ($\mathcal{O}(k^{n-1})$ or $\mathcal{O}(k^n)$).

In many cases the end user is only interested in a subset of states in a reachability analysis as opposed to the full reachability set. Because of this, it is useful to only compute the reachability set of the subspace that contains the states of interest. In this way, only the computational cost of the subspace of interest is incurred as opposed to the computational cost due to the full description of the reachability set. Holzinger et al. demonstrated application of the transversality conditions on sampled individual trajectories to allow subspace reachability set computation with significantly lower dimensionality-driven costs.[12] In addition, applying the necessary conditions of optimality, dynamics constraints, and initial condition constraints, a point solution of the subspace extremum surface may be used to find nearby solutions. Using this continuation approach and an initial state that satisfies the constraints, the computation of a point solution on the subspace extremum surface is reduced to an initial value problem solvable through numerical integration. The required computation under this proposed approach exponentially reduces from the problem dimension to the subspace dimension ($\mathcal{O}(k^{n-1}) \rightarrow \mathcal{O}(k^{s-1})$ where $1 \leq s \leq n$). As a result, a large variety of previously intractable reachability problems become computationally feasible.

The expected contributions from this research include: 1) The formulation of the optimal control policy and continuation method approach for subspaces while addressing numerical issues such as ill-conditioned constraint surface dynamics and numerical integration error. 2) Demonstration of proposed approach for computation of two-dimensional position reachability subspace for a spacecraft in Keplerian motion under multiple orbit regimes which only requires a one-dimensional exploration.

THEORY

Hamilton Jacobi Bellman PDE

An optimal reachability problem is defined as a continuum of Optimal Control Problems (OCPs) with initial conditions satisfying an inequality constraint on the initial value function $V(\boldsymbol{x}, t_0) \leq 0$. The Optimal Control Problem is formally stated as

$$\begin{aligned} \sup_{\boldsymbol{u} \in U} \left[\int_{t_0}^{t_f} \mathcal{L}(\boldsymbol{x}(\tau), \boldsymbol{u}(\tau), \tau) d\tau + V(\boldsymbol{x}_f, t_f) \right] & \\ \dot{\boldsymbol{x}} = \boldsymbol{f}(\boldsymbol{x}, \boldsymbol{u}, t) & \\ \boldsymbol{h}(\boldsymbol{x}, t) \leq \boldsymbol{0} & \\ \boldsymbol{g}(\boldsymbol{x}_0, t_0, \boldsymbol{x}_f, t_f) = \boldsymbol{0} & \end{aligned} \tag{1}$$

where $\boldsymbol{x} \in \mathbb{R}^n$ is the state, $\boldsymbol{u} \in \mathbb{R}^m$ is the control input, $t \in [t_0, t_f]$ is time, $\mathcal{L} : \mathbb{R}^n \times \mathbb{R}^m \times \mathbb{R} \rightarrow \mathbb{R}$ is the trajectory Lagrangian, $V : \mathbb{R}^n \times \mathbb{R} \rightarrow \mathbb{R}$ is the terminal performance function, $\boldsymbol{f} : \mathbb{R}^n \times \mathbb{R}^m \times \mathbb{R} \rightarrow \mathbb{R}^n$ captures the system differential equations, $\boldsymbol{h} : \mathbb{R}^n \times \mathbb{R} \rightarrow \mathbb{R}^q$ defines trajectory inequality constraints, $\boldsymbol{g} : \mathbb{R}^n \times \mathbb{R} \times \mathbb{R}^n \times \mathbb{R} \rightarrow \mathbb{R}^v$ expresses boundary conditions, and $U \subseteq \mathbb{R}^m$ defines the set of admissible controls. The admissible control set U is typically defined as

$$U = \{\boldsymbol{u} \mid \boldsymbol{u}^T \boldsymbol{u} \leq u_m^2\} \tag{2}$$

where $u_m \in \mathbb{R}^+$. This definition of the admissible control set is assumed for the remainder of this paper. Rearranging Eq. (1) into differential form yields the traditional HJB PDE as follows

$$\frac{\partial V}{\partial t} + \sup_{\boldsymbol{u} \in U} \Big[\mathcal{L}(\boldsymbol{x}, \boldsymbol{u}, \boldsymbol{p}, t) + \boldsymbol{p}^T \boldsymbol{f}(\boldsymbol{x}, \boldsymbol{u}, t) \Big] = 0 \tag{3}$$

where the adjoint variable $\boldsymbol{p}$ is the value function gradient with respect to the state and the second term in Eq. (3), denoted by $\mathcal{H}(\boldsymbol{x}, \boldsymbol{u}, \boldsymbol{p}, t)$, is called the Hamiltonian as it shares the same properties of the canonically defined Hamiltonian.

Commonly, minimum time reachability analyses are performed. In this case, the trajectory term $\mathcal{L}(\boldsymbol{x}, \boldsymbol{u}, \boldsymbol{p}, t) = 1$. The minimum time HJB PDE is then reduced as

$$\frac{\partial V}{\partial t} + \sup_{\boldsymbol{u} \in U} \Big[\boldsymbol{p}^T \boldsymbol{f}(\boldsymbol{x}, \boldsymbol{u}, t) \Big] = 0 \tag{4}$$

This is the form of the HJB PDE that will be used in this subspace reachability problem demonstration of this paper.

Subspace Reachability Formulation for Minimum Time

To avoid unnecessary computational cost by calculating the full state reachability manifold, the reachability computation is performed on a subspace $\mathbb{R}^s$ of the full state space $\mathbb{R}^n$ ($\mathbb{R}^s \subseteq \mathbb{R}^n$). This can be performed by decomposing the full state into the subspace of interest and residual subspace such that $\boldsymbol{x} = [\boldsymbol{x}_s^T \ \boldsymbol{x}_r^T]^T$. This reduces the dimensionality of the problem which leads to exponential improvement in computational tractability and complexity ($\mathcal{O}(k^{n-1}) \rightarrow \mathcal{O}(k^{s-1})$ where $1 \leq s \leq n$).

To compute points on the subspace reachability manifold after an amount of time, the final subspace distance must be maximized in a direction of interest in the given subspace.[12] This approach is analogous to the weighted L_p method in multi-objective optimization.[13] A search direction in $\mathbb{R}^s$ can be described using $\hat{\boldsymbol{d}}_s = \boldsymbol{R}(\boldsymbol{\theta})\hat{\boldsymbol{e}}_1$, where $\boldsymbol{R}(\boldsymbol{\theta}) \in \mathbb{R}^{s \times s}$ is an $s \times s$ right handed orthonormal rotation matrix parametrized by the rotation $\boldsymbol{\theta} \in \mathrm{SO}(s-1)$ and $\hat{\boldsymbol{e}}_1$ is the unit vector in the direction of the first state in $\boldsymbol{x}_{s,f}$.

The squared distance of the final state $\boldsymbol{x}_f$ along the search direction $\hat{\boldsymbol{d}}_s$ is

$$\boldsymbol{x}_{s,f}^T \hat{\boldsymbol{d}}_s \hat{\boldsymbol{d}}_s^T \boldsymbol{x}_{s,f} = \boldsymbol{x}_{s,f}^T \boldsymbol{R}(\boldsymbol{\theta}) \hat{\boldsymbol{e}}_1 \hat{\boldsymbol{e}}_1^T \boldsymbol{R}(\boldsymbol{\theta})^T \boldsymbol{x}_{s,f} \tag{5}$$

It is then possible to construct the performance index for a point solution on the subspace extremum surface as

$$V(\boldsymbol{x}_{s,f}, t_f, \boldsymbol{\theta}) = \frac{1}{2} \boldsymbol{x}_{s,f}^T \boldsymbol{R}(\boldsymbol{\theta}) \boldsymbol{D} \boldsymbol{R}(\boldsymbol{\theta})^T \boldsymbol{x}_{s,f} = \frac{1}{2} \boldsymbol{x}_{s,f}^T \boldsymbol{G} \boldsymbol{x}_{s,f} \tag{6}$$

where $\boldsymbol{D} = \hat{\boldsymbol{e}}_1 \hat{\boldsymbol{e}}_1^T$. For minimum time reachability without inequality constraints, the OCP given by Eqn. (1) then reduces to

$$\begin{aligned} \sup_{\boldsymbol{u}\in U} \frac{1}{2}\boldsymbol{x}_f^T \begin{bmatrix} \boldsymbol{G}_{s\times s} & \boldsymbol{0}_{s\times r} \\ \boldsymbol{0}_{r\times s} & \boldsymbol{0}_{r\times r} \end{bmatrix} \boldsymbol{x}_f \\ \dot{\boldsymbol{x}} = \boldsymbol{f}(\boldsymbol{x}, \boldsymbol{u}, t) \\ g(\boldsymbol{x}_0, t_0) = 0 \end{aligned} \tag{7}$$

where s is the dimension of the subspace of interest, $\boldsymbol{G} \in \mathbb{S}^{s\times s}$ is symmetric matrix, and $g(\boldsymbol{x}_0, t_0) = V(\boldsymbol{x}_0, t_0) = 0$ where $V(\boldsymbol{x}_0, t_0)$ is an initial boundary condition defined by the problem. An ellipsoid can be specified as the initial boundary of the reachability set as follows

$$V(\boldsymbol{x}_0, t_0) = \boldsymbol{x}_0^T \boldsymbol{E} \boldsymbol{x}_0 - 1 = 0 \tag{8}$$

where $\boldsymbol{E} \in \mathbb{S}^+_{n\times n} > 0$, is a symmetric positive definite matrix and $\boldsymbol{x}_0$ is the initial state. Ellipsoidal initial reachability sets are useful because they can represent the set of states that exist within a level set of a Gaussian probability density function. These probability ellipsoids can be generated from the estimate error covariance from typical estimation algorithms such as minimum variance estimators or batch filters.[14]

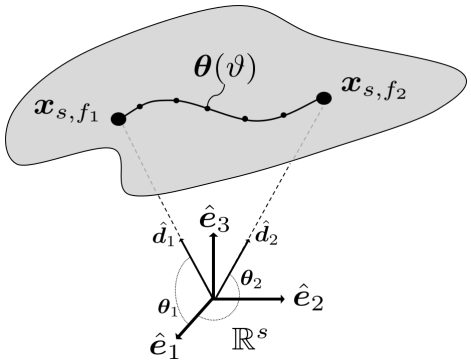


Figure 1. Search Direction Illustration

Each of the final states $\boldsymbol{x}_f$ are solutions to the optimal control problem (7) and compose the optimal reachability set. By choosing $g(\boldsymbol{x}_0, t_0) = V(\boldsymbol{x}_0, t_0) = 0$, the initial states of optimal trajectories lie on the surface of the initial reachability set. Maximizing the final distance subject to the OCP constraints is equivalent to finding a trajectory to the final distance in minimum time. Since the optimal control policy $\boldsymbol{u}^*(\boldsymbol{x}(t), \boldsymbol{p}(t))$ is known, the optimal $\boldsymbol{x}_f^*$ can be acquired by optimizing Eq. (6) in a given search direction parametrized by $\boldsymbol{\theta}$. Figure 1 visualizes the idea of parameterizing the final point solutions $\boldsymbol{x}_{s,f}$ to the subspace reachability problem using the rotation parameter $\boldsymbol{\theta}$.

Continuation Methods

Applying the transversality conditions to the subspace OCP defined in (7) the following boundary conditions on the adjoints of a given optimal trajectory are written as

$$\boldsymbol{p}_0 = -\frac{\partial V}{\partial \boldsymbol{x}_0} - \lambda \frac{\partial g}{\partial \boldsymbol{x}_0} = -\lambda \frac{\partial g}{\partial \boldsymbol{x}_0} \tag{9}$$

$$\boldsymbol{p}_f = \frac{\partial V}{\partial \boldsymbol{x}_f} + \lambda \frac{\partial g}{\partial \boldsymbol{x}_f} = \begin{bmatrix} \boldsymbol{G}\boldsymbol{x}_{s,f} \\ \boldsymbol{0}_{r\times 1} \end{bmatrix} \tag{10}$$

where $\lambda \in \mathbb{R}$ is the Lagrange multiplier corresponding to the initial condition constraint $g(\boldsymbol{x}_0, t_0)$.

As the final time horizon, $t_f = t_0 + T$, is chosen, specific values of $\boldsymbol{x}_0(T)$ and $\lambda(T)$ can be found to maximize (6). After applying the transversality constraints, the optimal state $\boldsymbol{x}^*$ and adjoint $\boldsymbol{p}^*$ along the optimal trajectory can be combined into the constraint

$$\boldsymbol{\kappa}(\boldsymbol{x}_0^*(T), \boldsymbol{p}_0^*(T), \lambda^*(T), \boldsymbol{\theta}) = \mathbf{0} \tag{11}$$

enforcing the full state dynamics and necessary conditions of optimality.[12]

After applying the necessary conditions of optimality, dynamics constraints, and initial condition constraints, a point solution of the subspace extremum surface may be used to find nearby solutions.[12] Combining the full state $\boldsymbol{x}$ and Lagrange multiplier λ into a parameter state $\boldsymbol{z} \in \mathbb{R}^{n+1}$ and defining an independent parameter $\vartheta \in \mathbb{R}$, moving along the constraint surfaces satisfies

$$\frac{d\boldsymbol{\kappa}}{d\vartheta} = \frac{\partial \boldsymbol{\kappa}(\vartheta)}{\partial \boldsymbol{z}} \frac{d\boldsymbol{z}(\vartheta)}{d\vartheta} + \frac{\partial \boldsymbol{\kappa}(\vartheta)}{\partial \vartheta} = \mathbf{0} \tag{12}$$

After rearranging the terms, if $\partial\boldsymbol{\kappa}/\partial\boldsymbol{z}$ is left-invertible, the parameter dynamics along the constraint surface $\boldsymbol{\kappa}(\boldsymbol{z}(\vartheta), \vartheta)$ as ϑ changes are described by the first-order nonlinear differential equation

$$\frac{d\boldsymbol{z}(\vartheta)}{d\vartheta} = -\left[\frac{\partial \boldsymbol{\kappa}(\vartheta)}{\partial \boldsymbol{z}}\right]^{-1} \left(\frac{\partial \boldsymbol{\kappa}(\vartheta)}{\partial \vartheta}\right) = \boldsymbol{M}^{-1}\boldsymbol{b} \tag{13}$$

where $\boldsymbol{M}$ represents the Jacobian matrix of the constraints with respect to the parameter state $\boldsymbol{z}$ and $\boldsymbol{b}$ represents the dynamics of the constraints with respect to the independent parameter ϑ. Using this concept, Holzinger et al.[12] has shown that the unique first order differential equation that represents the motion of $\boldsymbol{x}_0(T)$ and $\lambda(T)$ along the optimal trajectory constraint surface is given as

$$\begin{bmatrix} \frac{d\boldsymbol{x}_0}{dT} \\ \frac{d\lambda}{dT} \end{bmatrix} = \begin{bmatrix} \frac{\partial \boldsymbol{\kappa}_1}{\partial \boldsymbol{x_0}} & \frac{\partial \boldsymbol{\kappa}_1}{\partial \lambda} \\ \frac{\partial \boldsymbol{\kappa}_2}{\partial \boldsymbol{x_0}} & 0 \end{bmatrix}^{-1} \begin{bmatrix} \begin{bmatrix} \boldsymbol{G} & \mathbf{0} \\ \mathbf{0} & \mathbf{0} \end{bmatrix} \dot{\boldsymbol{x}} - \dot{\boldsymbol{p}} \\ 0 \end{bmatrix} \tag{14}$$

where $T = t_f - t_0$ is the time horizon over which the reachability set is computed, $\boldsymbol{\kappa}_1(\boldsymbol{x}_0(T), \lambda(T)) = \mathbf{0}_{n\times 1}$ represents the equality constraint for transversality conditions, and $\kappa_2(\boldsymbol{x}_0(T)) = 0$ represents the equality constraint for the initial condition constraint $g(\boldsymbol{x}_0(T), t_0)$. Using this continuation approach and an initial state $\boldsymbol{z}_0(T) = [\boldsymbol{z}_0^T(T) \quad \lambda^T(T)]^T$ that satisfies the constraints contained in $\boldsymbol{\kappa}$, the exploration of the subspace extremum surface is reduced to an initial value problem solvable through numerical integration.

Potential Numerical Issues

Depending on the constraint dynamics and scale between the coordinates of the initial parameter state $\boldsymbol{z}_0$, as T increases the numerical condition number of $\boldsymbol{M}$ may increase arbitrarily. In numerical linear algebra, the condition number of a matrix, denoted in this paper as $\tilde{\kappa}(\boldsymbol{M})$, gives a measure of the sensitivity of the solution to the general linear system $\boldsymbol{My} = \boldsymbol{b}$.[15] As $\tilde{\kappa}(\boldsymbol{M})$ from (14) increases, the accuracy of the solution may decrease. As a general rule of thumb, if the condition number $\tilde{\kappa}(\boldsymbol{M})$ is on the order of 10^k then it is possible to lose up to k digits of accuracy in the solution to a given linear system.[15]

To maintain a specified level of accuracy in the constraint dynamics, a maximum allowable absolute tolerance in the solution can be set. In many numerical integrator routines, such as ode45 in MATLAB, an absolute tolerance ($AbsTol$) can be specified to bound the largest acceptable solver error. Additionally, the numerical accuracy of the integrated solution will be limited by the precision of the floating point numbers used. For example, using double-precision floating-point format numbers will result in approximately 16 decimal digits ($\log_{10} 2^{52} \approx 15.65$). As a result, the following condition may be set on the condition number $\tilde{\kappa}(\boldsymbol{M})$

$$\log_{10}(AbsTol) + \log_{10}(\tilde{\kappa}(\boldsymbol{M})) \leq log_{10}\left(\frac{1}{10^k\ \epsilon}\right) \tag{15}$$

which simplifies to the following conservative upper bound on $\tilde{\kappa}(\boldsymbol{M})$

$$\log_{10}(\tilde{\kappa}(\boldsymbol{M})) \leq log_{10}\left(\frac{AbsTol}{10^k\ \epsilon}\right) \tag{16}$$

where k is the user-specified number of accurate decimal digits in the integrator solution and ϵ is the numerical precision of the digital number format (such as 2^{-52} for double-precision numbers). This condition (16) can be used in the numerical integration routine that solves (14) as a terminal condition or a trigger to modify the integration tolerances.

Dynamics

This approach of exploring the reachability subspace is demonstrated on the case of a spacecraft in Keplerian orbit with maximum thrust constraints where only the orbital planar motion is considered. As such, the full state of the system will be described by two position and two velocity states.

While the condition above describes the conservative upper bound on $\tilde{\kappa}(\boldsymbol{M})$, it is possible to reduce $\tilde{\kappa}(\boldsymbol{M})$ through scaling time and distance in the dynamics or change of units. For example, describing the inertial position and velocity of an object near GEO requires the position scale ($\|\boldsymbol{r}\| \approx$ 42164 km) to be approximately 4 orders of magnitude larger than the velocity scale ($\|\boldsymbol{v}\| \approx 3$ km/s) when SI units are used. To better condition the dynamics, it is possible to scale time and scale such that the first and second order variations of the state coordinates are on the same order of magnitude. If the new time coordinate $s = \alpha t$ and $\tilde{x} = \gamma x$ with $\alpha, \gamma \in \mathbb{R}^+$, then the scaled dynamics for a single variable are be rewritten as follows

$$\mathring{\tilde{x}} = \frac{d\tilde{x}}{ds} = \frac{d(\gamma x)}{dt} \cdot \frac{dt}{ds} = \frac{\gamma}{\alpha}\dot{x}\ ,\ \ \mathring{\mathring{\tilde{x}}} = \frac{d^2\tilde{x}}{ds^2} = \frac{\gamma}{\alpha^2}\ddot{x} \tag{17}$$

Depending on the initial state dynamics, α can then be chosen to be used in (17) to appropriately scale the first and second variations of the state in the new time coordinate s such that $\boldsymbol{M}$ is better conditioned. A convenient choice of α is $1/n$ where n is the mean motion of the object in orbit. This choice of α results in a full orbit period $P = 2\pi$ in the scaled time units. Similarly, scaling the spatial dimensions could also help alleviate numerical conditioning issues for the proposed approach. Another alternative to improve the conditioning of $\tilde{\kappa}(\boldsymbol{M})$ is to utilize a change of units. For example, describing the inertial position and velocity of an object near GEO requires the position scale ($\|\boldsymbol{r}\| \approx 6.6$ DU) to be approximately 1 order of magnitude larger than the velocity scale ($\|\boldsymbol{v}\| \approx 0.4$ DU/TU) when Earth canonical units are used.[16]

The exact nonlinear relative equations of motion for a spacecraft about a given arbitrary reference orbit $\boldsymbol{x}_r(t)$ are

$$\dot{\boldsymbol{x}} = \begin{bmatrix} \dot{x} \\ \dot{y} \\ \ddot{x} \\ \ddot{y} \end{bmatrix} = \begin{bmatrix} \dot{x} \\ \dot{y} \\ 2\dot{f}_r\big(\dot{y} - y\frac{\dot{r}_r}{r_r}\big) + x\dot{f}_r^2 + \frac{\mu}{r_r^2} - \frac{\mu}{r^3}(r_r + x) + u_x \\ -2\dot{f}_r\big(\dot{x} - x\frac{\dot{r}_r}{r_r}\big) + y\dot{f}_r^2 - \frac{\mu}{r^3}y + u_y \end{bmatrix} \tag{18}$$

where the true anomaly rate $(\dot{f}_r)$, reference radius (r_r), and reference radius time derivative $(\dot{r}_r)$ can be directly computed using Keplerian dynamics and the inertial radius of the spacecraft is r, defined as $r = \sqrt{(r_r + x)^2 + y^2}$.[16] Because the motion in the z direction is weakly coupled with the x and y motion, the problem is restricted to motion in the x and y directions, causing $\boldsymbol{x}_0 \in \mathbb{R}^4$. These equations of motion represent the relative motion between a spacecraft and a reference object in a reference orbit. The dynamics are expressed in a rotating Hill frame, where the radial axis (x) points from the center of the Earth to the reference object and the along-track axis (y) is defined as perpendicular to the radial vector and is positive in the direction of the reference orbit velocity.

If both time and position are scaled such that $s = \alpha t$, $\tilde{x} = \gamma x$, and $\tilde{y} = \gamma y$, the scaled exact nonlinear relative equations of motion for a spacecraft about a given reference orbit $\boldsymbol{x}_r(t)$ are

$$\mathring{\tilde{\boldsymbol{x}}} = \frac{d\tilde{\boldsymbol{x}}}{ds} = \begin{bmatrix} \mathring{\tilde{x}} \\ \mathring{\tilde{y}} \\ \mathring{\mathring{\tilde{x}}} \\ \mathring{\mathring{\tilde{y}}} \end{bmatrix} = \begin{bmatrix} \mathring{\tilde{x}} \\ \mathring{\tilde{y}} \\ \frac{\gamma}{\alpha^2}\left(2\frac{\alpha^2}{\gamma}\mathring{f}_r\big(\mathring{\tilde{y}} - \frac{1}{\gamma}\tilde{y}\frac{\mathring{\tilde{r}}_r}{\tilde{r}_r}\big) + \frac{\alpha^2}{\gamma}\tilde{x}\mathring{f}_r^2 + \gamma^2\frac{\tilde{\mu}}{\tilde{r}_r^2} - \gamma^2\frac{\tilde{\mu}}{\tilde{r}^3}(\tilde{r}_r + \tilde{x}) + \tilde{u}_x\right) \\ \frac{\gamma}{\alpha^2}\left(-2\frac{\alpha^2}{\gamma}\mathring{f}_r\big(\mathring{\tilde{x}} - \frac{1}{\gamma}\tilde{x}\frac{\mathring{\tilde{r}}_r}{\tilde{r}_r}\big) + \frac{\alpha^2}{\gamma}\tilde{y}\mathring{f}_r^2 - \gamma^2\frac{\tilde{\mu}}{\tilde{r}^3}\tilde{y} + \tilde{u}_y\right) \end{bmatrix} \tag{19}$$

where $\tilde{r}_r = \gamma r_r$, $\mathring{\tilde{r}}_r = \frac{\gamma}{\alpha} r_r$, $\tilde{r} = \gamma r$, $\tilde{\mu} = \frac{\gamma^3}{\alpha^2}\mu$, $\tilde{u}_x = \frac{\gamma}{\alpha^2}u_x$, and $\tilde{u}_y = \frac{\gamma}{\alpha^2}u_y$. For the results generated in this paper, α is set to $1/n$ where n is mean motion and the distance scale is unchanged $(\gamma = 1)$.

RESULTS

This approach of exploring the reachability subspace is demonstrated on the case of a spacecraft in Keplerian orbit with maximum thrust constraints where only planar motion is considered. The two-dimensional position subspace reachability manifold is then computed using Eq. (4) and the outlined methodology. As the reachability set for the two-dimensional subspace is explored with a one-dimensional search (θ), these examples demonstrate subspace reachability calculations with computations $\mathcal{O}(k)$ as opposed to $\mathcal{O}(k^4)$ or $\mathcal{O}(k^3)$. In addition to demonstrating the generation of the position subspace reachability set for two dimensions, this example demonstrates the capability to compute the reachability set boundaries under nonlinear dynamics.

The initial reachability set represented by $V(\boldsymbol{x}_0, t_0)$ is chosen to be defined by the ellipsoidal constraint

$$V(\boldsymbol{x}_0, t_0) = \begin{bmatrix} \boldsymbol{d}_0 \\ \boldsymbol{v}_0 \end{bmatrix}^T \begin{bmatrix} \frac{1}{r_d^2}\mathbb{I} & \mathbf{0}_{2\times2} \\ \mathbf{0}_{2\times2} & \frac{1}{r_v^2}\mathbb{I} \end{bmatrix} \begin{bmatrix} \boldsymbol{d}_0 \\ \boldsymbol{v}_0 \end{bmatrix} - 1 = 0$$

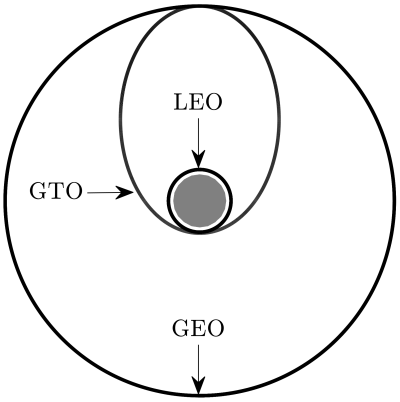


Figure 2. Orbital Geometry of LEO, GTO, and GEO

with r_d set to 1 m and r_v set to 0.1 m/s.

The following examples demonstrate the 2D minimum time position reachability set calculation over 3 different orbital regimes: Low Earth Orbit (LEO), Geostationary transfer orbit (GTO), and Geostationary orbit (GEO). The chosen reference orbits are all equatorial with the reference object starting at perigee at t_0. The control has an upper bound of $u_m = 2e^{-5}$ m/s^2, which is equivalent to a 500 kg spacecraft with a 0.01 N thruster. In using Eqn. (7), the search direction $\hat{\boldsymbol{d}}_s(\theta)$ is varied within the x-y plane over $[0, 2\pi]$ at samplings sufficient enough to generate detailed surfaces.

For each of the following orbit regimes, the subspace reachability set is computed for up to half an orbit period. At this point for each of the cases, the problem becomes numerically ill-conditioned. By altering the values of the dynamics scaling using α and γ, subspace reachability set computations at longer time horizons are possible.

LEO Orbit

The chosen reference orbit is an equatorial circular low Earth orbit (LEO) with an altitude of 400 km. Fig. 3 shows the maximal position subspace reachability set and associated optimal trajectories in the Hill frame after one half orbit period of about 46.2 minutes.

Fig. 4 shows the same LEO position reachability set evolve with time as $t_f = [\frac{1}{8}P, \frac{1}{4}P, \frac{3}{8}P, \frac{1}{2}P]$.

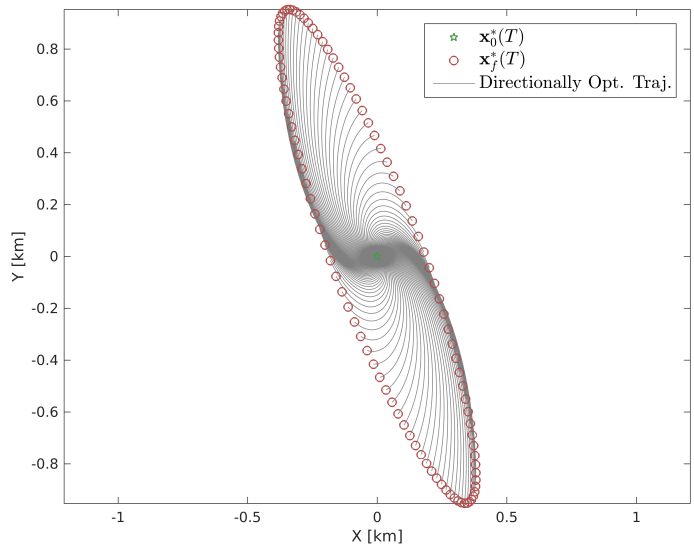


Figure 3. Position-reachability set for 2-DOF nonlinear relative Keplerian motion in rotating Hill frame - LEO Orbit

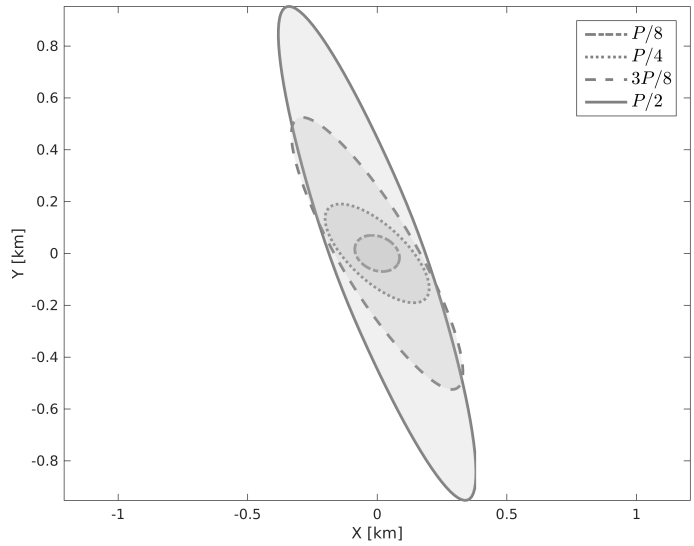


Figure 4. Position-reachability set for 2-DOF nonlinear relative Keplerian motion at times $t_f = [\frac{1}{8}P, \frac{1}{4}P, \frac{3}{8}P, \frac{1}{2}P]$ in rotating Hill frame - LEO Orbit

GEO Orbit

The chosen reference orbit is an equatorial circular geostationary orbit (GEO) with an altitude of 35786 km. Fig. 5 shows the maximal position subspace reachability set and associated optimal trajectories in the Hill frame after one half orbit period of 12 hours.

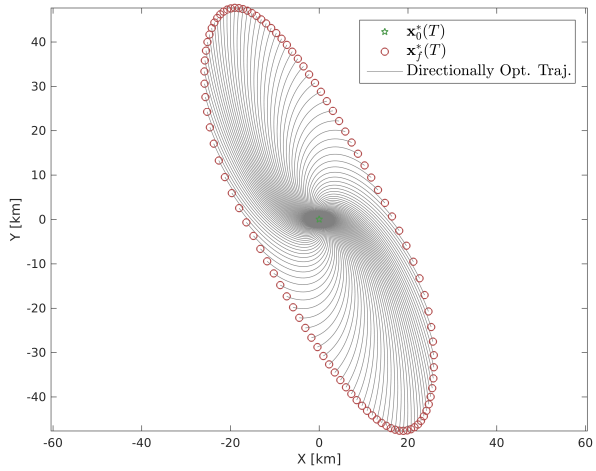


Figure 5. Position-reachability set for 2-DOF nonlinear relative Keplerian motion in rotating Hill frame - GEO Orbit

Fig. 6 shows the same GEO position reachability set evolve with time as $t_f = [\frac{1}{8}P, \frac{1}{4}P, \frac{3}{8}P, \frac{1}{2}P]$.

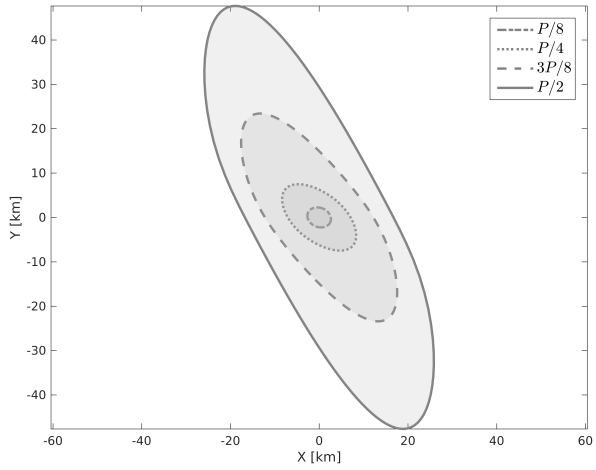


Figure 6. Position-reachability set for 2-DOF nonlinear relative Keplerian motion at times $t_f = [\frac{1}{8}P, \frac{1}{4}P, \frac{3}{8}P, \frac{1}{2}P]$ in rotating Hill frame - GEO Orbit

GTO Orbit

The chosen reference orbit is in an equatorial geostationary transfer orbit with a perigee radius of 7000 km and a apogee at GEO altitude of 35786 km. Fig. 7 shows the maximal position subspace reachability set and associated optimal trajectories in the Hill frame after one half orbit period of about 5.33 hours.

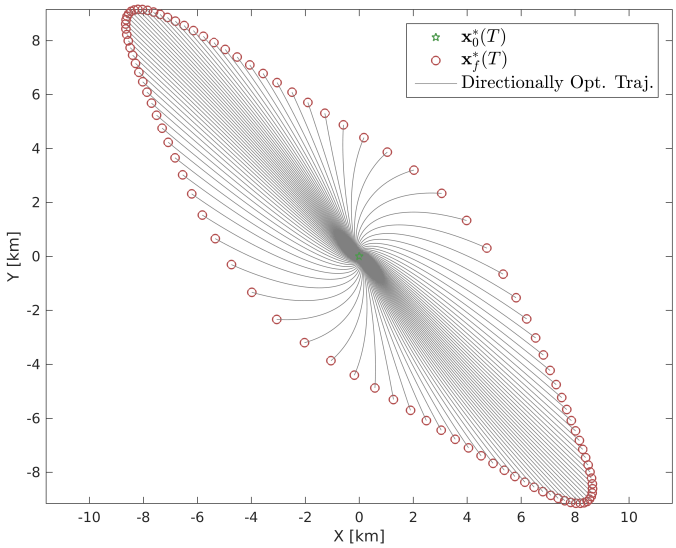


Figure 7. Position-reachability set for 2-DOF nonlinear relative Keplerian motion in rotating Hill frame - GTO Orbit

Fig. 8 shows the same GTO position reachability set evolve with time as $t_f = [\frac{1}{8}P, \frac{1}{4}P, \frac{3}{8}P, \frac{1}{2}P]$.

In general, as T increases, dense or sparse densities of point solutions may form on the reachability surface. To better describe the reachability set at a given time horizon, it is possible to insert additional trajectories to generate additional point solutions. This is performed by searching for the largest point-wise distances along the boundary of the reachability set and identifying which initial search directions encompass this region. Then additional $\hat{\boldsymbol{d}}_s(\theta)$ can be inserted into the grid by bisecting the neighboring initial search directions. This technique of binary discretization refinement is demonstrated at the final time horizon of the GTO case in Fig. 9. Fig. 10 shows how large point-wise distances can be lessened in the subspace reachability set at a given time horizon through the introduction of these bisecting search directions.

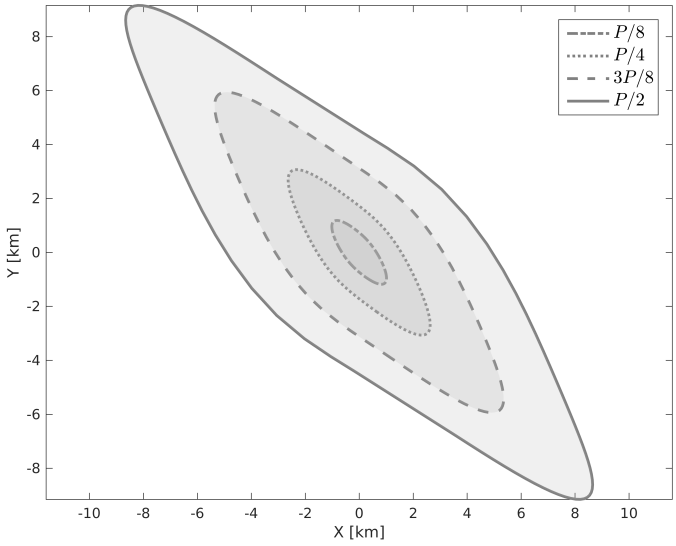


Figure 8. Position-reachability set for 2-DOF nonlinear relative Keplerian motion at times $t_f = [\frac{1}{8}P, \frac{1}{4}P, \frac{3}{8}P, \frac{1}{2}P]$ in rotating Hill frame - GTO Orbit

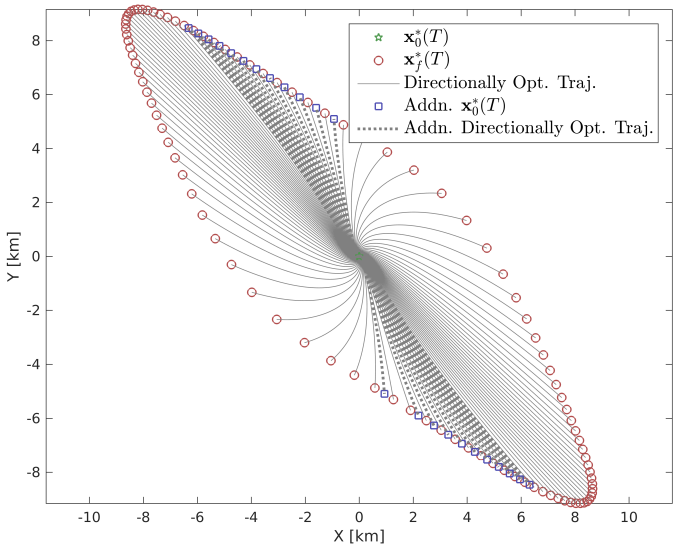
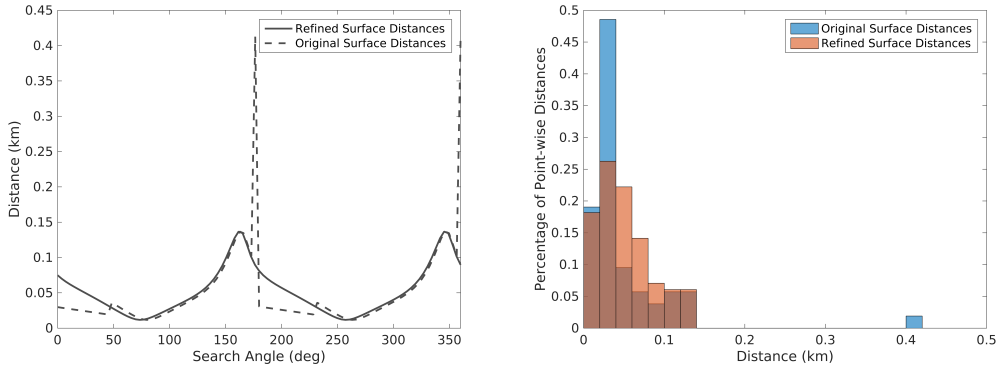


Figure 9. Position-reachability set for 2-DOF nonlinear relative Keplerian motion in rotating Hill frame with binary discretization refinement - GTO Orbit



(a) Point-wise distance in reachable position subspace with and without surface refinement

(b) Histogram of distances between point solutions with and without surface refinement

Figure 10. Visualization of binary discretization refinement

CONCLUSIONS AND FUTURE WORK

By sampling the initial reachability subspace, it is shown that the reachability subspace after a given time horizon T may be found by numerically integrating the constraint surface dynamics with computation time $\mathcal{O}(k^{s-1})$. This approach of exploring the reachability subspace using continuation methods is demonstrated with the case of a spacecraft in Keplerian orbit with maximum thrust constraints. Reduction in computation load is achieved as the reachability manifold is computed for only the two position states as opposed to the full four dimensional state. This reduces the subspace reachability problem into a one-dimension exploration, exponentially reducing the computational cost from $\mathcal{O}(k^3) \rightarrow \mathcal{O}(k)$. Potential numerical issues that may arise due to the conditioning of the constraint dynamics are introduced and numerical techniques to better condition the problem are discussed. Future work will focus on the potential numerical issues such as cusps and concavities that can arise if a final state $\boldsymbol{x}_f^*(T)$ is reachable from multiple initial conditions $\boldsymbol{x}_0^*(T)$. Further comparisons are to be made between this approach and alternate reachability solution methods such as viscosity methods[4] in terms of computation load and accuracy of the position subspace extremum surface. Additionally, future work includes a further investigation into the numerical scaling of the problem as well as incorporating ΔV costs for constrained time and fuel reachability.

ACKNOWLEDGEMENTS

This work is supported by the NASA Space Technology Research Fellowship Grant No. NNX16AM39H.

REFERENCES

[1] P. Varaiya, "Reach Set Computation Using Optimal Control," *Proc. KIT Workshop*, 1997, pp. 377–383.

[2] J. Lygeros, "On Reachability and Minimum Cost Optimal Control," *Automatica*, Vol. 40, June 2004, pp. 917–927, doi:10.1016/j.automatica.2004.01.012.

[3] A. B. Kurzhanski and P. Varaiya, "Dynamic Optimization for Reachability Problems," *Journal of Optimization Theory and Applications*, Vol. 108, No. 2, 2001, pp. 227–251, doi:10.1023/A:1026497115405.

[4] I. M. Mitchell, "A Toolbox of Level Set Methods," technical report, UBC Department of Computer Science, June 2007.

[5] A. M. Bayen and C. J. Tomlin, "A construction procedure using characteristics for viscosity solutions of the Hamilton-Jacobi equation," *Decision and Control, 2001. Proceedings of the 40th IEEE Conference on*, Vol. 2, 2001, pp. 1657–1662 vol.2, doi:10.1109/.2001.981139.

[6] J. Anderson, J. Degroote, G. Degrez, E. Dick, R. Grundmann, and J. Vierendeels, *Computational Fluid Dynamics: An Introduction*. Springer Berlin Heidelberg, 3 ed., 2009, doi:10.1007/978-3-540-85056-4.

[7] M. J. Holzinger, D. J. Scheeres, and J. Hauser, "Reachability Using Arbitrary Performance Indices," *IEEE Transactions on Automatic Control*, Vol. 60, Apr 2015, pp. 1099–1103, doi:10.1109/tac.2015.2391451.

[8] I. Hwang, D. M. Stipanović, and C. J. Tomlin, *Polytopic Approximations of Reachable Sets Applied to Linear Dynamic Games and a Class of Nonlinear Systems*, pp. 3–19. 2005, doi:10.1007/0-8176-4409-1.

[9] M. J. Holzinger and D. J. Scheeres, "Reachability Results for Nonlinear Systems with Ellipsoidal Initial Sets," *IEEE Transactions on Aerospace and Electronic Systems*, Vol. 48, April 2012, pp. 1583–1600, doi:10.1109/TAES.2012.6178080.

[10] A. Girard and C. L. Guernic, "Efficient Reachability Analysis for Linear Systems using Support Functions," *IFAC Proceedings Volumes*, Vol. 41, No. 2, 2008, pp. 8966–8971, doi:10.3182/20080706-5-kr-1001.01514.

[11] B. HomChaudhuri, M. Oishi, M. Shubert, M. Baldwin, and R. S. Erwin, "Computing reach-avoid sets for space vehicle docking under continuous thrust," *2016 IEEE 55th Conference on Decision and Control (CDC)*, Dec 2016, pp. 3312–3318, doi: 10.1109/CDC.2016.7798767.

[12] M. J. Holzinger and D. J. Scheeres, "Reachability set subspace computation for nonlinear systems using sampling methods," *IEEE Conference on Decision and Control and European Control Conference*, Institute of Electrical and Electronics Engineers (IEEE), Dec 2011, doi:10.1109/cdc.2011.6160728.

[13] K. Deb, *Multi-Objective Optimization Using Evolutionary Algorithms*. New York, NY, USA: John Wiley & Sons, Inc., 2001.

[14] A. Gelb, *Applied Optimal Estimation*. Cambridge, MA: MIT Press, 1974.

[15] L. N. Trefethen and D. B. III, *Numerical Linear Algebra*. SIAM: Society for Industrial and Applied Mathematics, June 1997.

[16] H. Schaub and J. L. Junkins, *Analytical Mechanics of Space Systems*. Reston, VA: AIAA Education Series, October 2003, 10.2514/4.861550.